15th RHESSI Workshop, 26-30 July 2016, Graz

DIFFUSIVE TRANSPORT OF ENERGETIC ELECTRONS IN THE 2004, MAY 21 SOLAR FLARE

Sophie Musset[1], Eduard Kontar[2], Nicole Vilmer[1]

[1] LESIA, Observatoire de Paris
[2] School of Physics and Astronomy, University of Glasgow

OUTLINE

1. RHESSI Imaging Spectroscopy: a new tool to study electron transport during solar flares
2. The 2004 May 21 solar flare
3. The diffusive transport model (Kontar et al, 2014)
4. Comparison between observations and model predictions
5. Conclusions

RHESSI IMAGING SPECTROSCOPY: A NEW TOOL TO STUDY ELECTRON TRANSPORT DURING FLARES

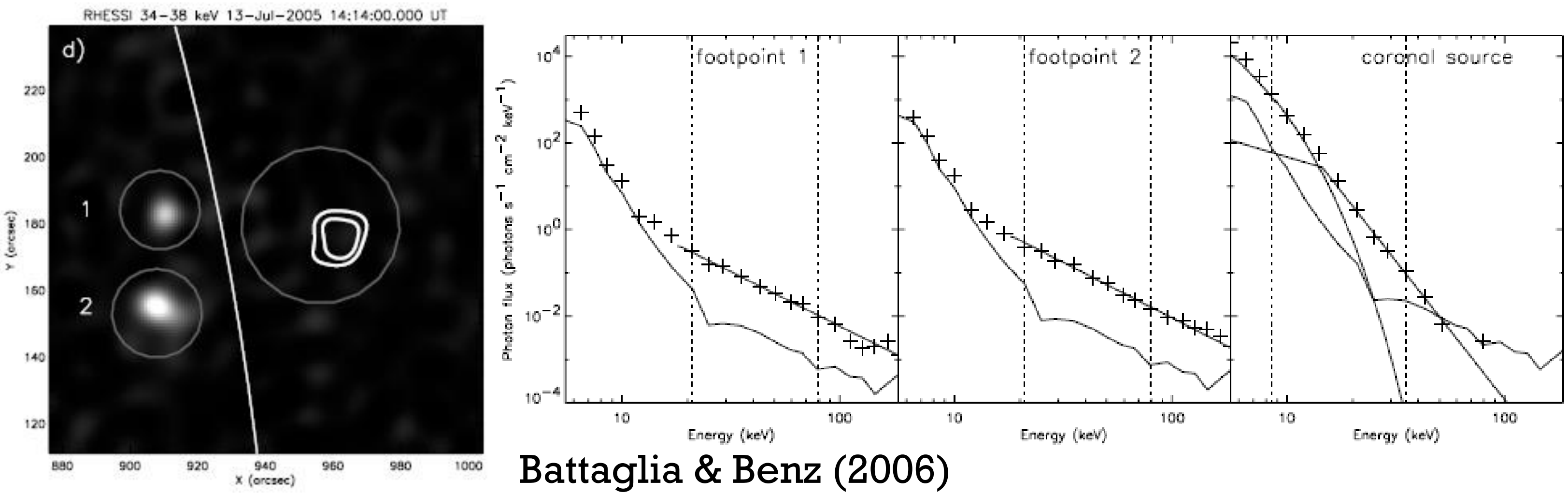

Battaglia & Benz (2006)

RHESSI IMAGING SPECTROSCOPY: A NEW TOOL TO STUDY ELECTRON TRANSPORT DURING FLARES

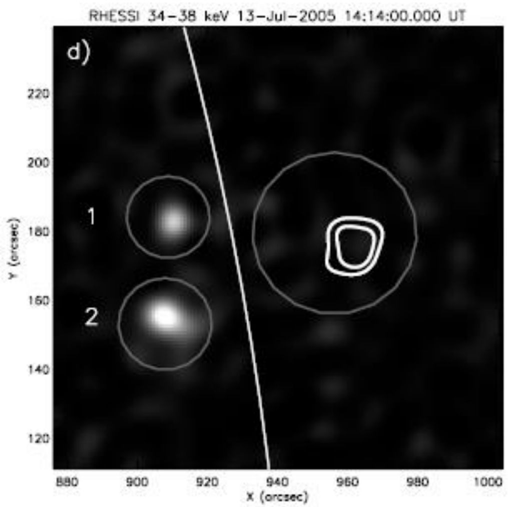

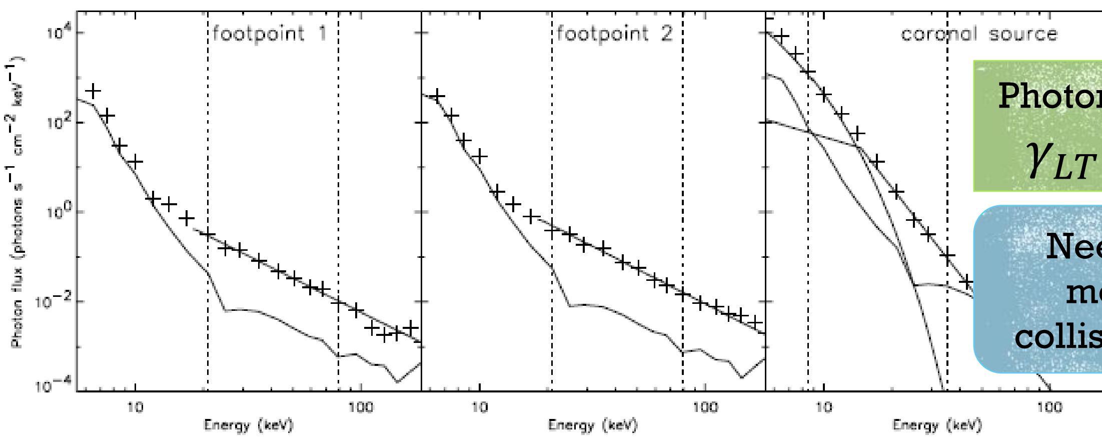

Battaglia & Benz (2006)

Photon spectral index
$$\gamma_{LT} - \gamma_{FP} \neq 2$$

Need additional mechanism to collisional transport

RHESSI IMAGING SPECTROSCOPY: A NEW TOOL TO STUDY ELECTRON TRANSPORT DURING FLARES

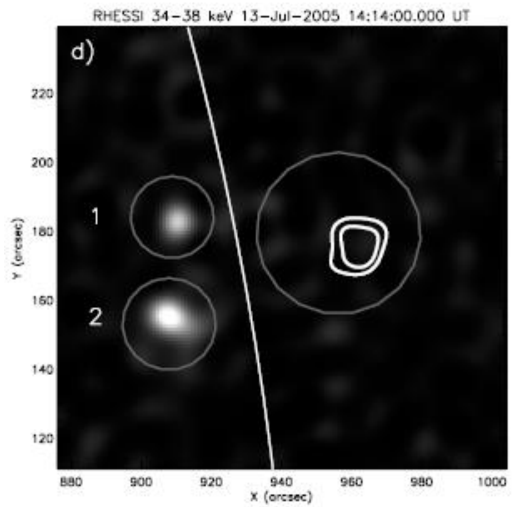

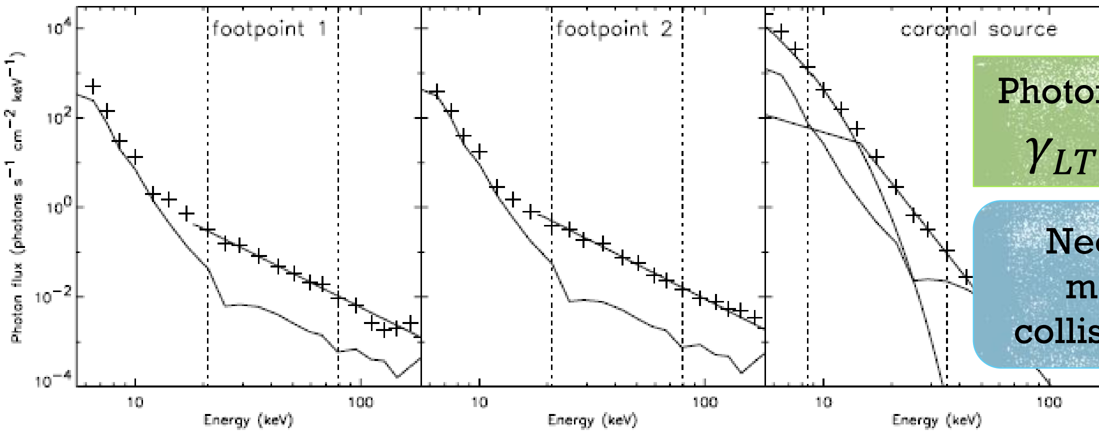

Battaglia & Benz (2006)

Photon spectral index

$$\gamma_{LT} - \gamma_{FP} \neq 2$$

Need additional mechanism to collisional transport

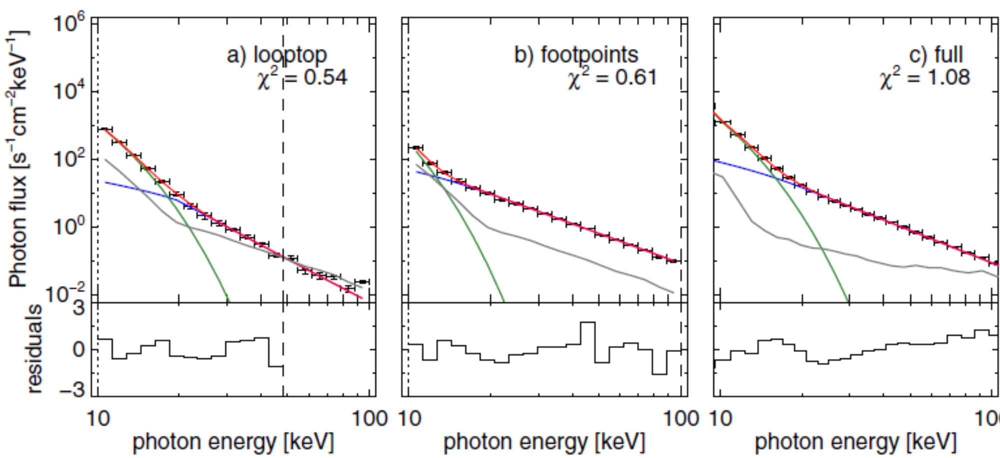

Simoes & Kontar (2013)

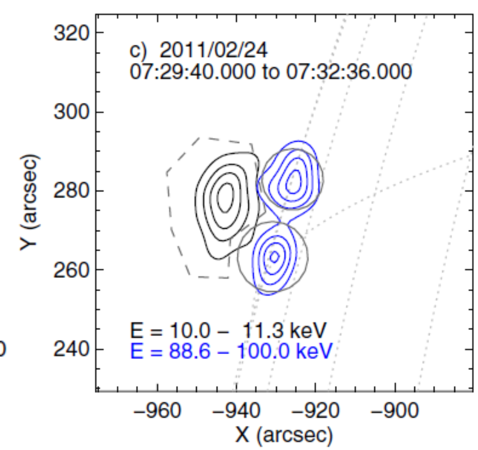

RHESSI IMAGING SPECTROSCOPY: A NEW TOOL TO STUDY ELECTRON TRANSPORT DURING FLARES

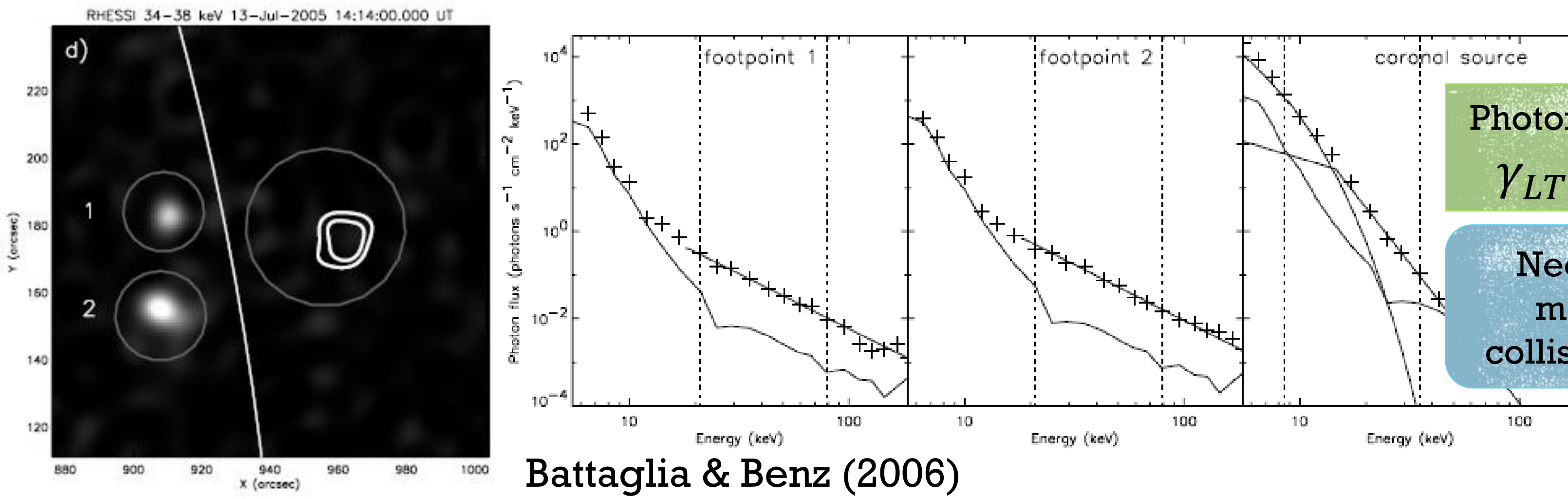

Battaglia & Benz (2006)

Photon spectral index

$$\gamma_{LT} - \gamma_{FP} \neq 2$$

Need additional mechanism to collisional transport

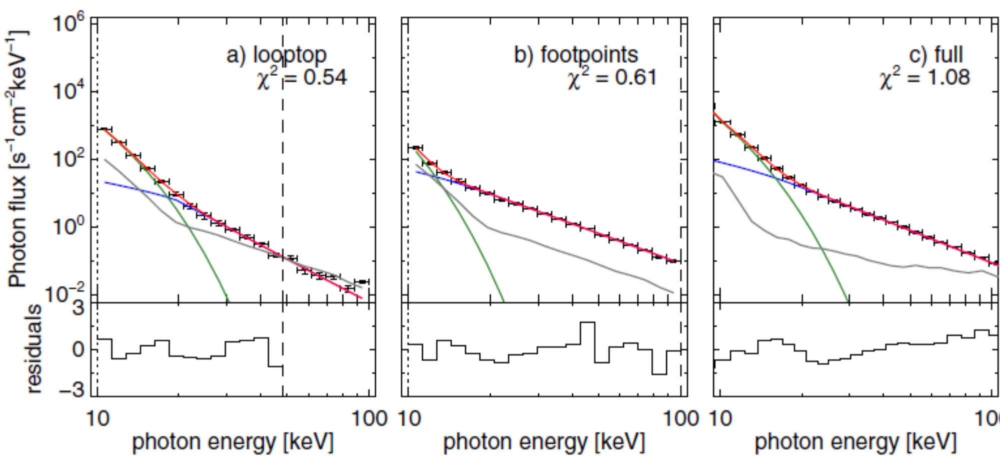

Simoes & Kontar (2013)

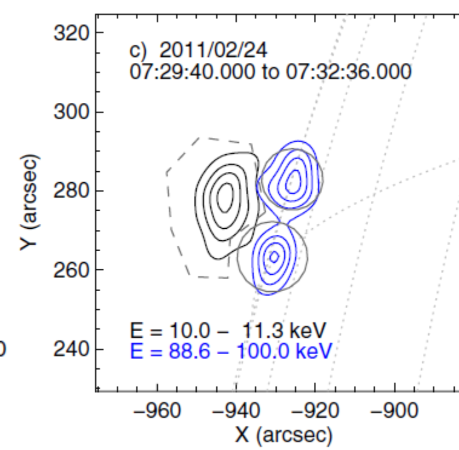

Electron spectral index

$$\delta_{LT} - \delta_{FP} < 0$$

Ratio of electron rate

$$\frac{\dot{N}_{LT}}{\dot{N}_{FP}} > 1$$

Need additional mechanism to collisional transport

THE 2004 MAY 21 SOLAR FLARE

Radio observations : Kuznetsov & Kontar (2015)

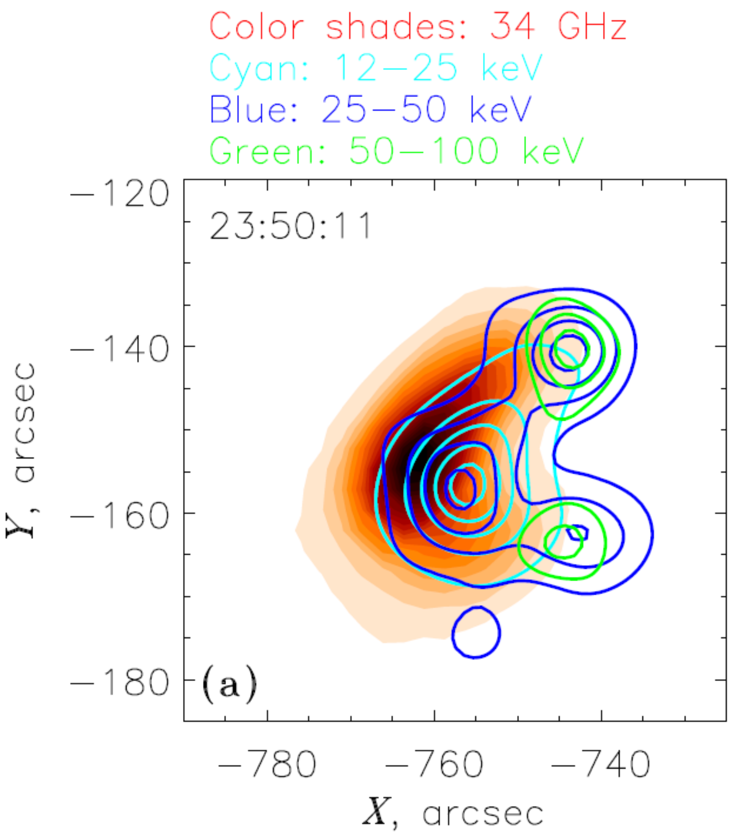

THE 2004 MAY 21 SOLAR FLARE

Radio observations : Kuznetsov & Kontar (2015)

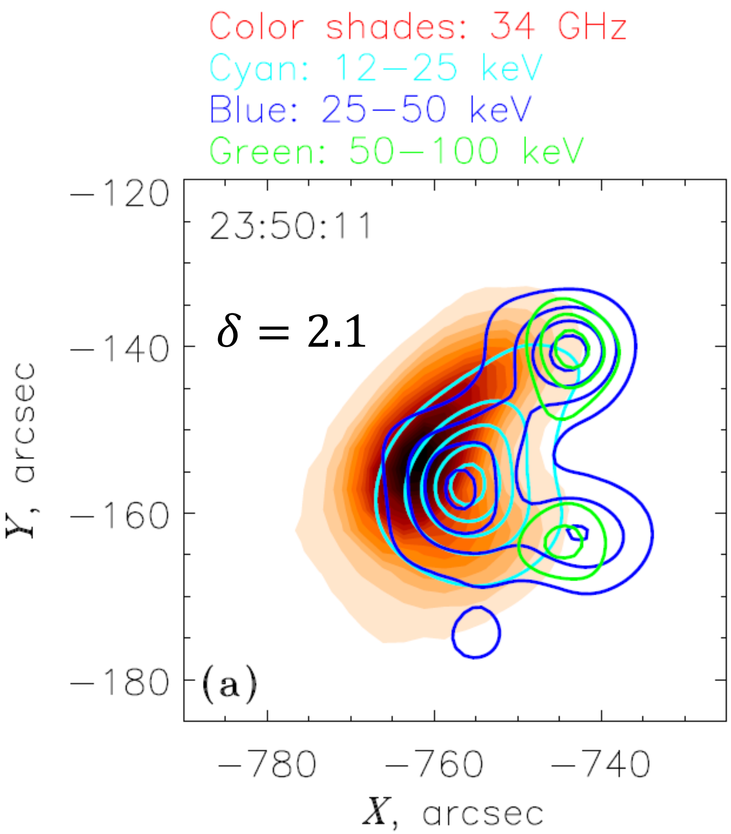

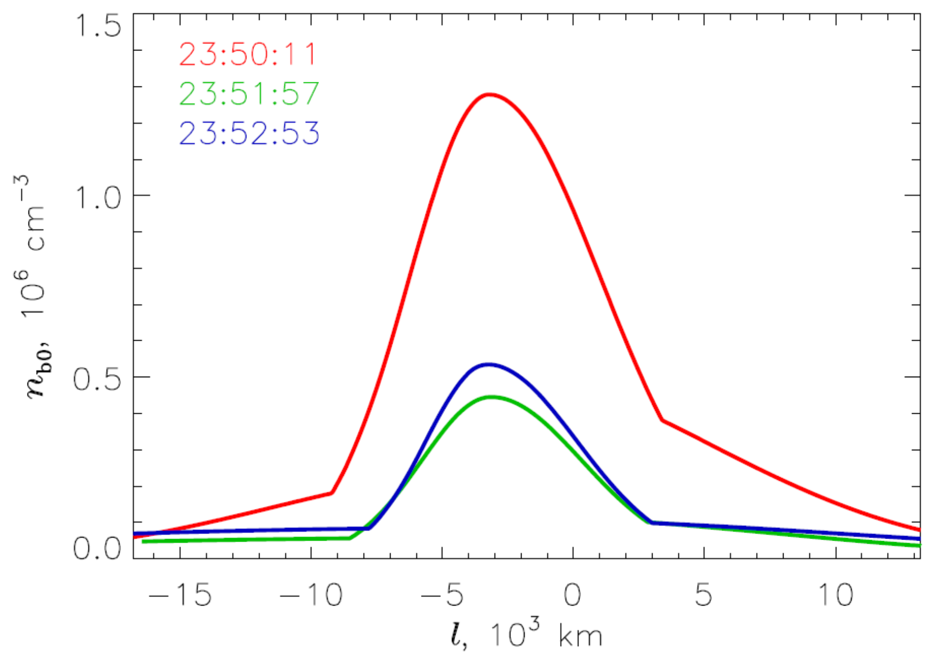

Spatial distribution of the density of energetic electrons with E > 60 keV

THE 2004 MAY 21 SOLAR FLARE

X-ray imaging spectroscopy
Musset et al, in prep

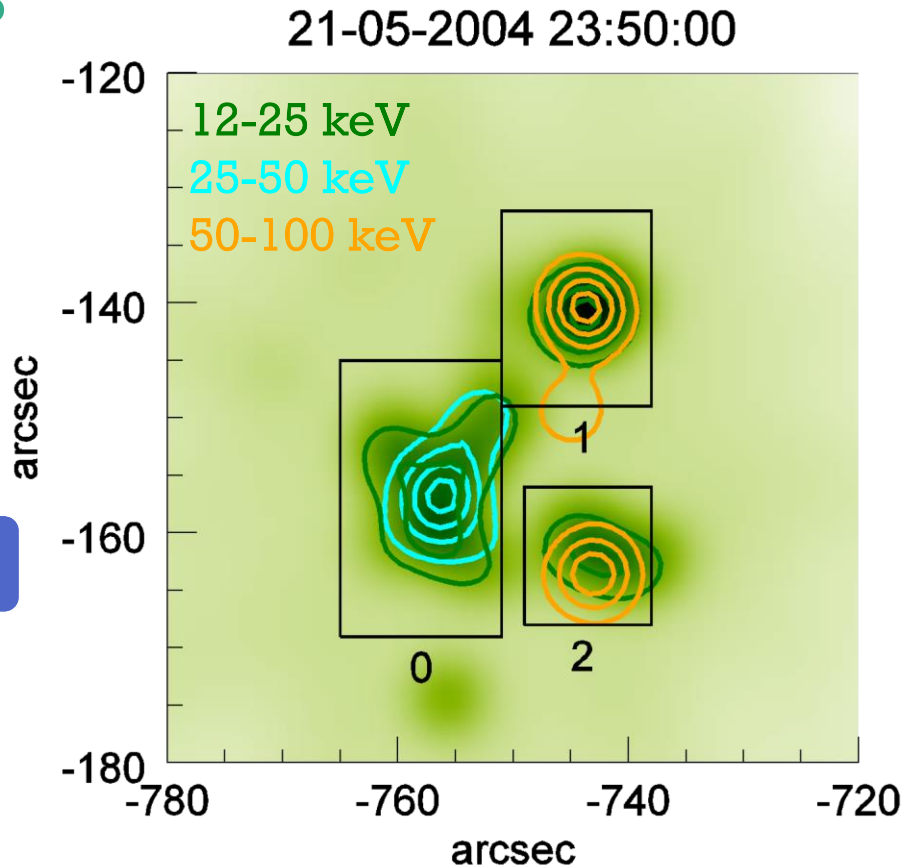

Thin target

Thick target

Thick target

THE 2004 MAY 21 SOLAR FLARE

X-ray imaging spectroscopy
Musset et al, in prep

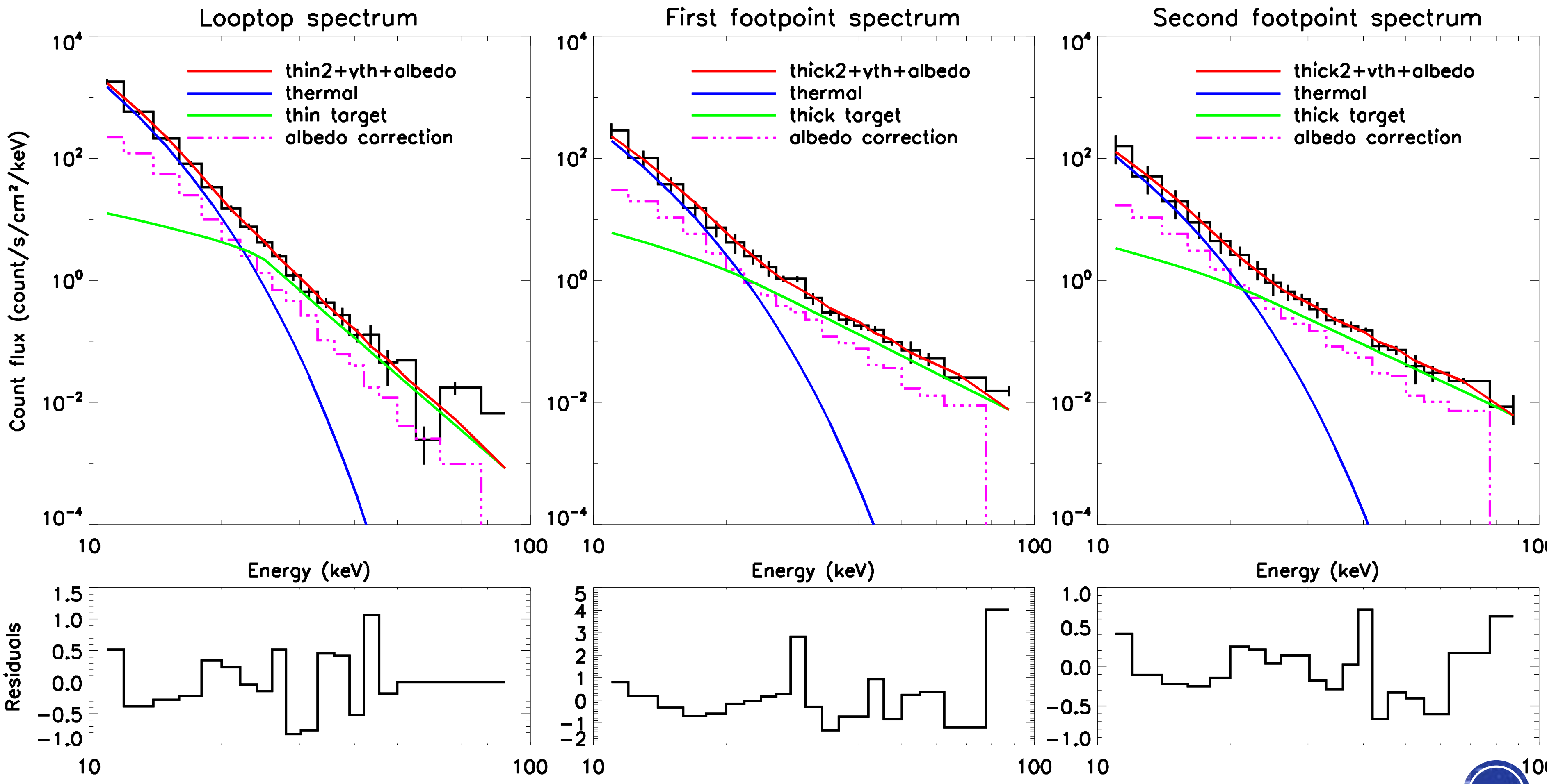

THE 2004 MAY 21 SOLAR FLARE

X-ray imaging spectroscopy
Musset et al, in prep

Thin target
Electron spectral index: δ
Integrated electron mean flux spectrum above E_0=25 keV
$$[nVF_0] = \int_{E_0}^{\infty} nVF(E)dE$$

$\delta = 5.2 \pm 0.4$
$[nVF_0] = 0.46 \pm 0.08 \times 10^{55}\ cm^{-2}s^{-1}$

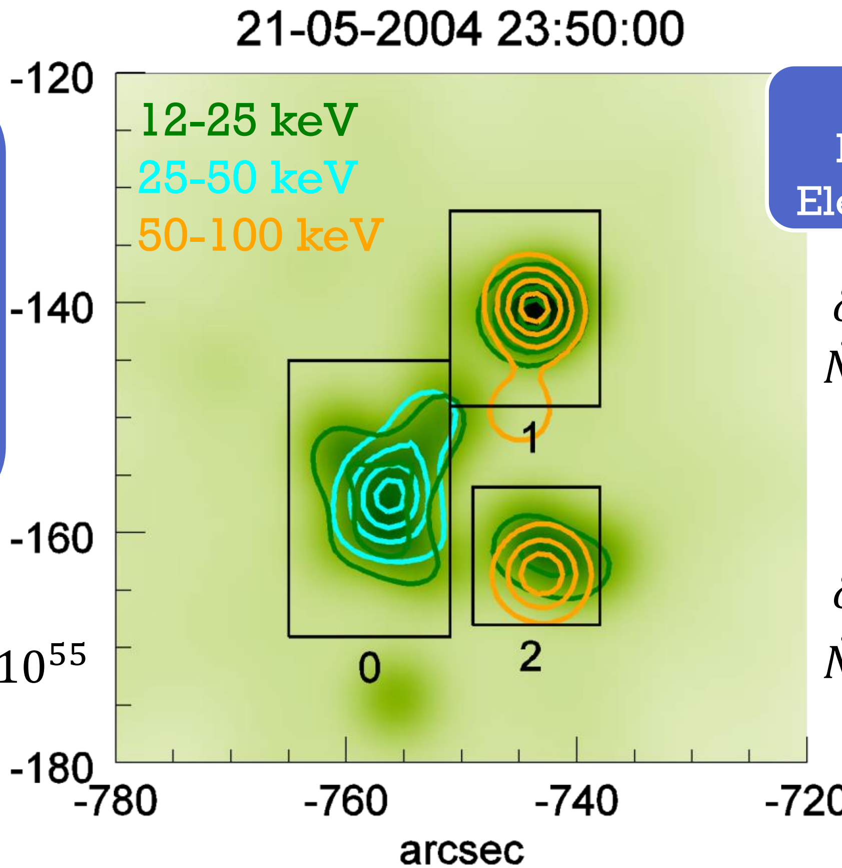

Thick target
Electron spectral index: δ
Electron rate above 25 keV: $\dot{N}$

$\delta = 4.4 \pm 0.2$
$\dot{N} = 0.12 \pm 0.03 \times 10^{35}\ s^{-1}$

$\delta = 4.2 \pm 0.2$
$\dot{N} = 0.06 \pm 0.02 \times 10^{35}\ s^{-1}$

THE 2004 MAY 21 SOLAR FLARE

X-ray imaging spectroscopy
Musset et al, in prep

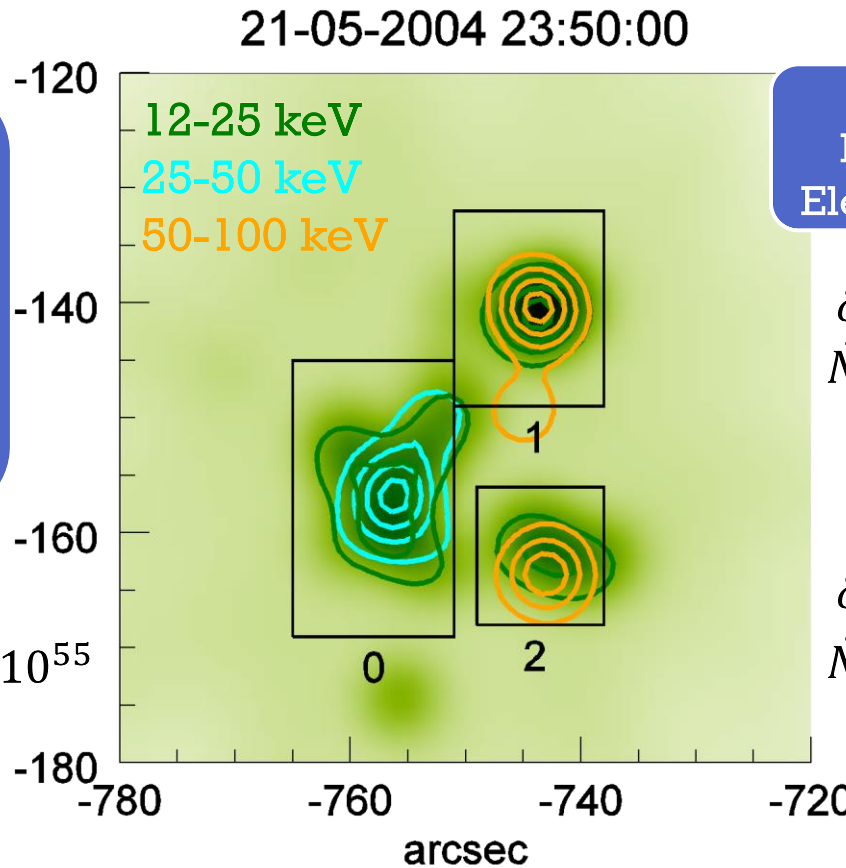

Thin target
Electron spectral index: δ
Integrated electron mean flux spectrum above E_0=25 keV

$$[nVF_0] = \int_{E_0}^{\infty} nVF(E)dE$$

$$\delta = 5.2 \pm 0.4$$

$$[nVF_0] = 0.46 \pm 0.08 \times 10^{55}\ cm^{-2}s^{-1}$$

Thick target
Electron spectral index: δ
Electron rate above 25 keV: $\dot{N}$

$$\delta = 4.4 \pm 0.2$$

$$\dot{N} = 0.12 \pm 0.03 \times 10^{35}\ s^{-1}$$

$$\delta = 4.2 \pm 0.2$$

$$\dot{N} = 0.06 \pm 0.02 \times 10^{35}\ s^{-1}$$

Distance between the footpoints and the looptop source: ~ 17 and $\sim 15 \times 10^8$ cm
➔ Length of the loop $L \sim 3.2 \times 10^9$ cm

THE 2004 MAY 21 SOLAR FLARE

X-ray imaging spectroscopy
Musset et al, in prep

$$\dot{N}_{LT} = A_{LT}\int_{E_0}^{\infty} F(E)dE = A_{LT}\int_{E_0}^{\infty}\frac{nVF(E)}{nV}dE$$

$$\dot{\boldsymbol{N}}_{\boldsymbol{LT}} = \frac{\mathbf{1}}{\boldsymbol{nL_{LT}}}\int_{\boldsymbol{E_0}}^{\infty}\boldsymbol{nVF(E)dE}$$

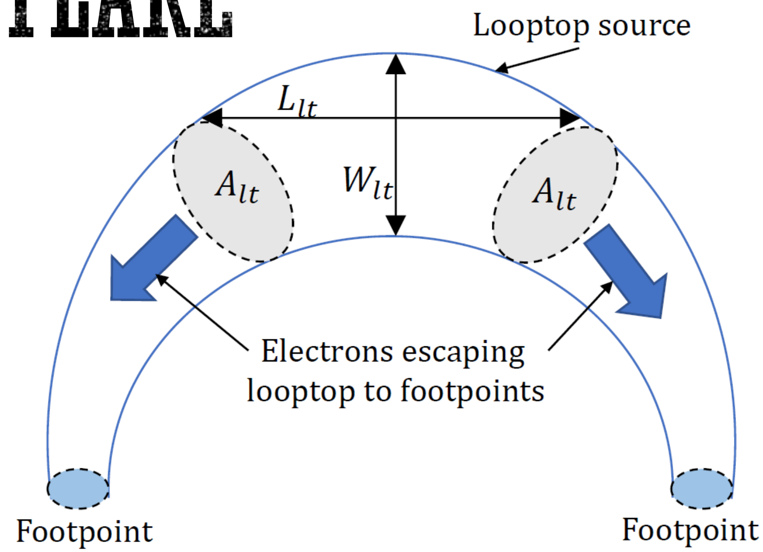

THE 2004 MAY 21 SOLAR FLARE

X-ray imaging spectroscopy
Musset et al, in prep

$$\dot{N}_{LT} = A_{LT}\int_{E_0}^{\infty} F(E)dE = A_{LT}\int_{E_0}^{\infty} \frac{nVF(E)}{nV}dE$$

$$\dot{\boldsymbol{N}}_{\boldsymbol{LT}} = \frac{\mathbf{1}}{\boldsymbol{nL_{LT}}}\int_{\boldsymbol{E_0}}^{\infty} \boldsymbol{nVF(E)dE}$$

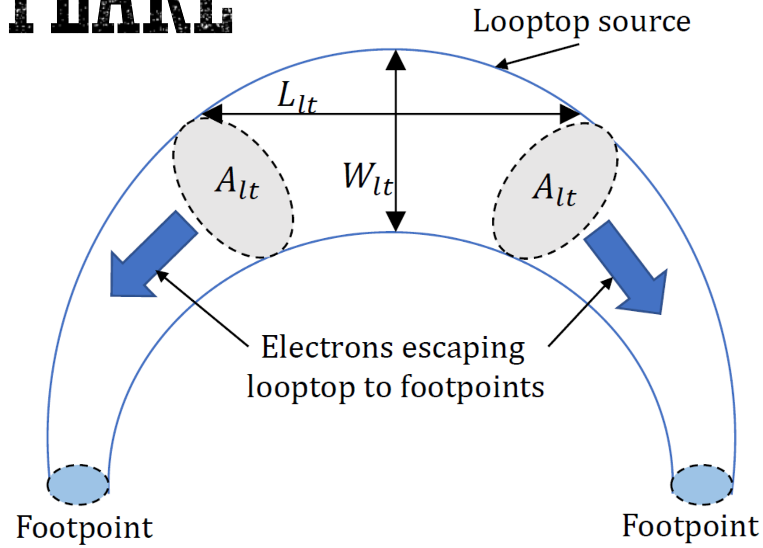

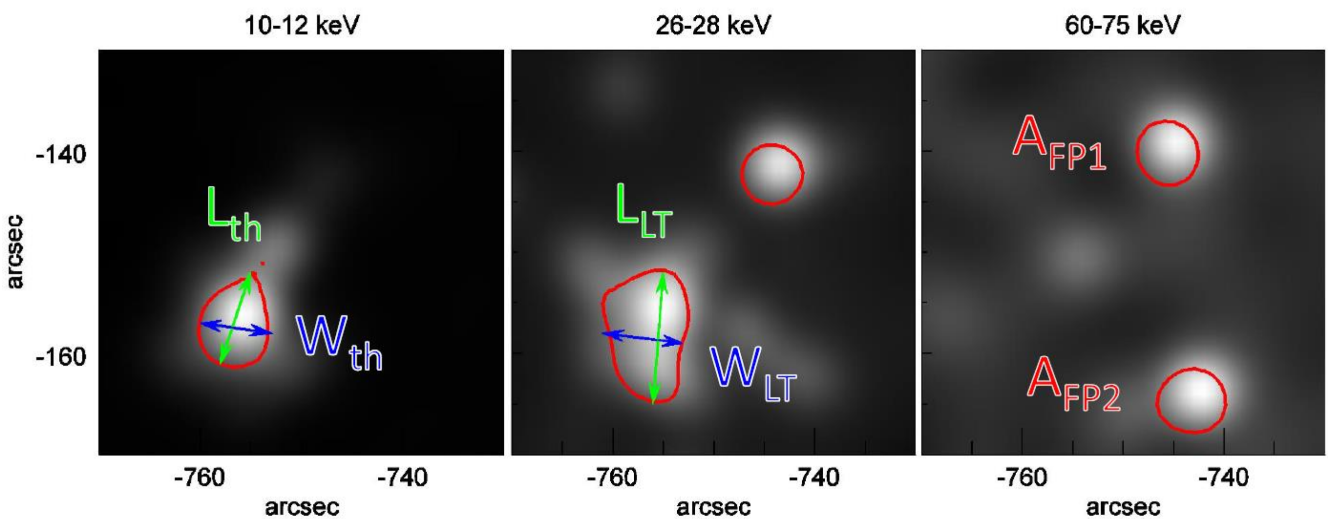

$$L_{LT} = 9.6 \times 10^{8}\ cm$$

$$V_{th} = 1.5 \times 10^{26}\ cm^{3}$$

$$n = \sqrt{EM/V_{th}}$$
$$= 1.2 \pm 0.2 \times 10^{11}\ cm^{-3}$$

$$\boxed{\dot{N}_{LT} = 0.4 \pm 0.2 \times 10^{35}\ s^{-1}}$$

$$\boxed{\frac{\dot{\boldsymbol{N}}_{\boldsymbol{LT}}}{\dot{\boldsymbol{N}}_{\boldsymbol{FP}}} = 2.2}$$

THE 2004 MAY 21 SOLAR FLARE

Spatial distribution of electrons
<nVF(E,z)> at 25 keV

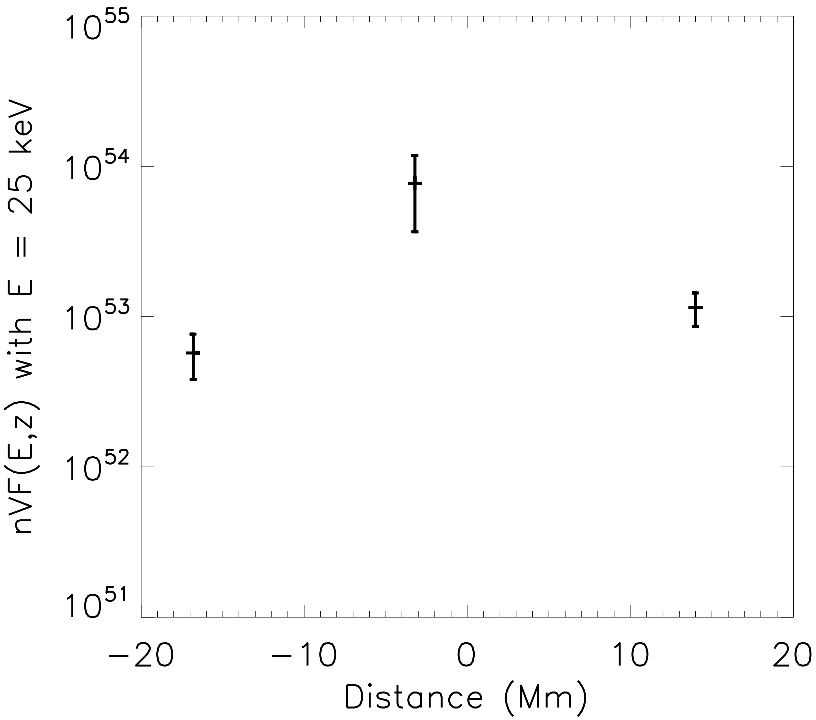

Electron mean spectra <nVF(E,z)>
in the different parts of the loop

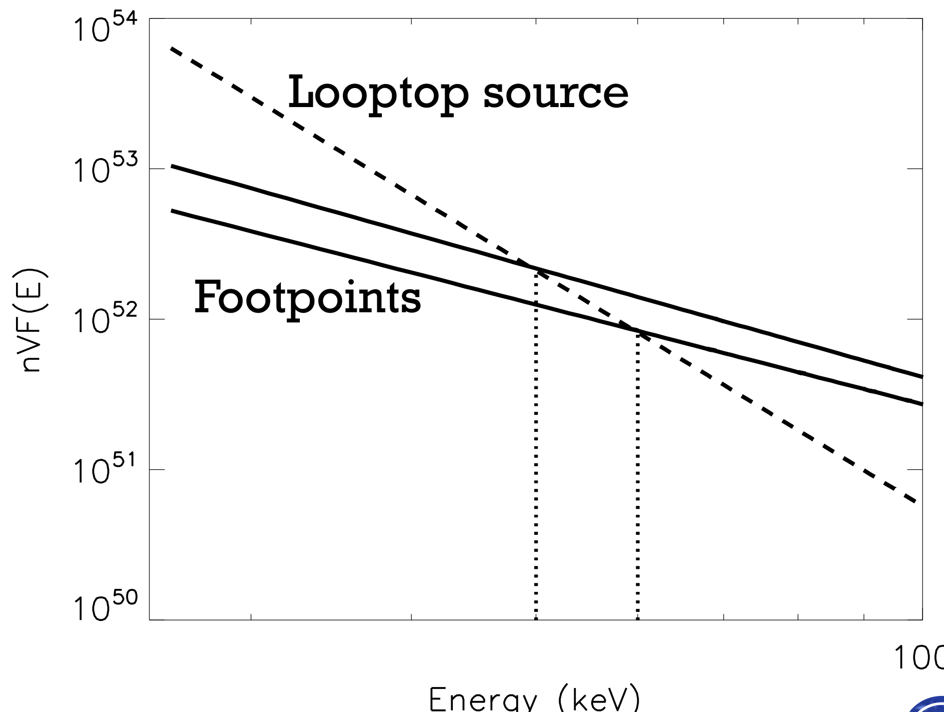

THE 2004 MAY 21 SOLAR FLARE

Energetic electron density above E_{min} $\qquad n_b^{E_{min}} = \int_{E_{min}}^{\infty} \frac{F(E)}{v(E)} dE \quad cm^{-3}$

Energetic electron density above 25 keV

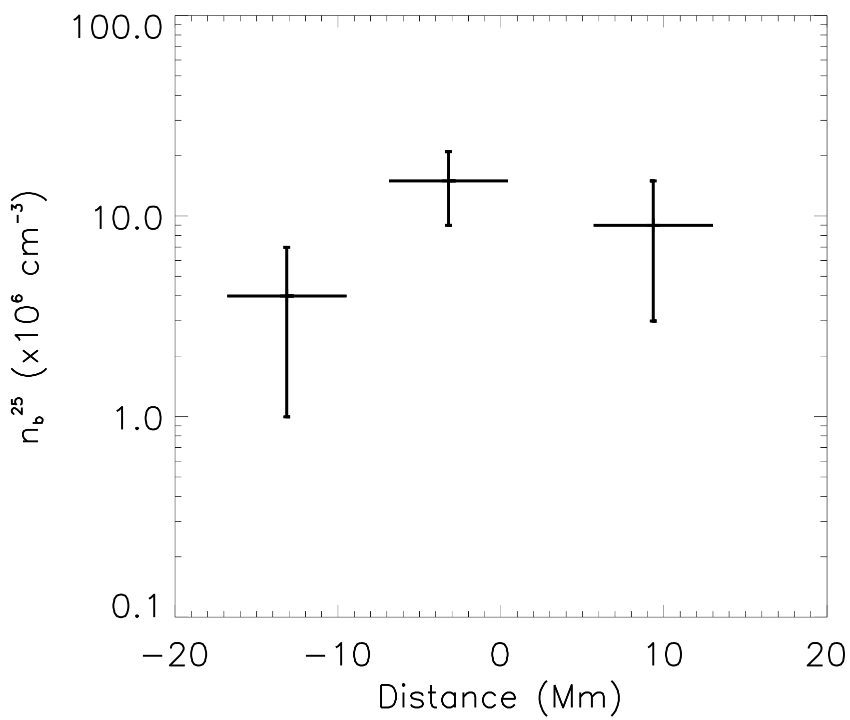

THE 2004 MAY 21 SOLAR FLARE

Energetic electron density above E_{min}

$$n_b^{E_{min}} = \int_{E_{min}}^{\infty} \frac{F(E)}{v(E)} dE \quad \text{cm}^{-3}$$

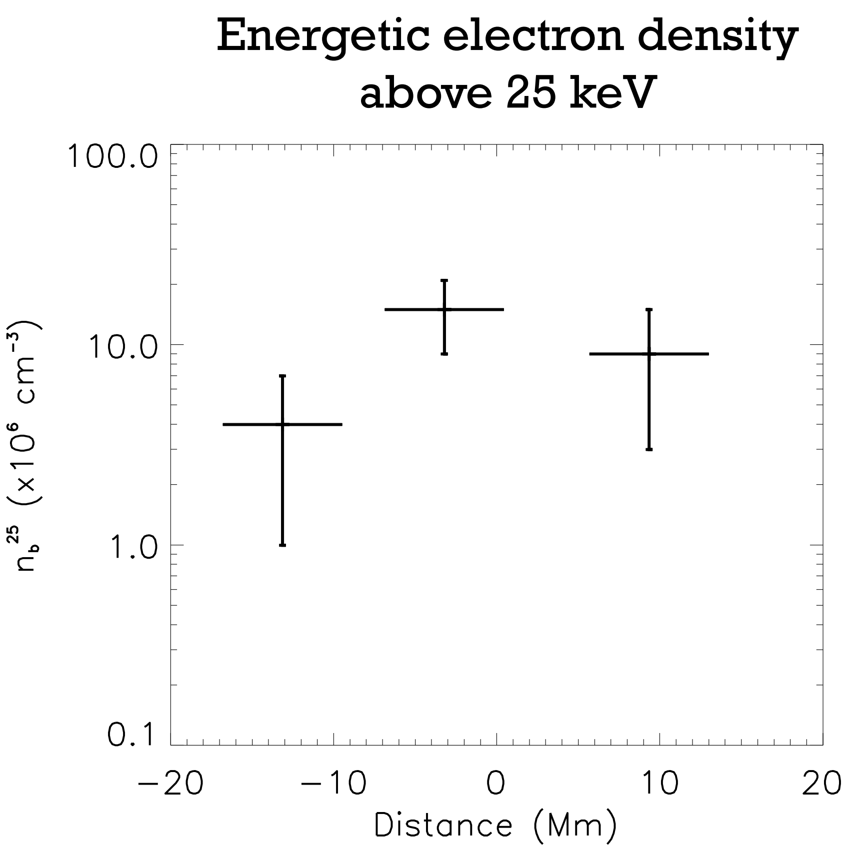

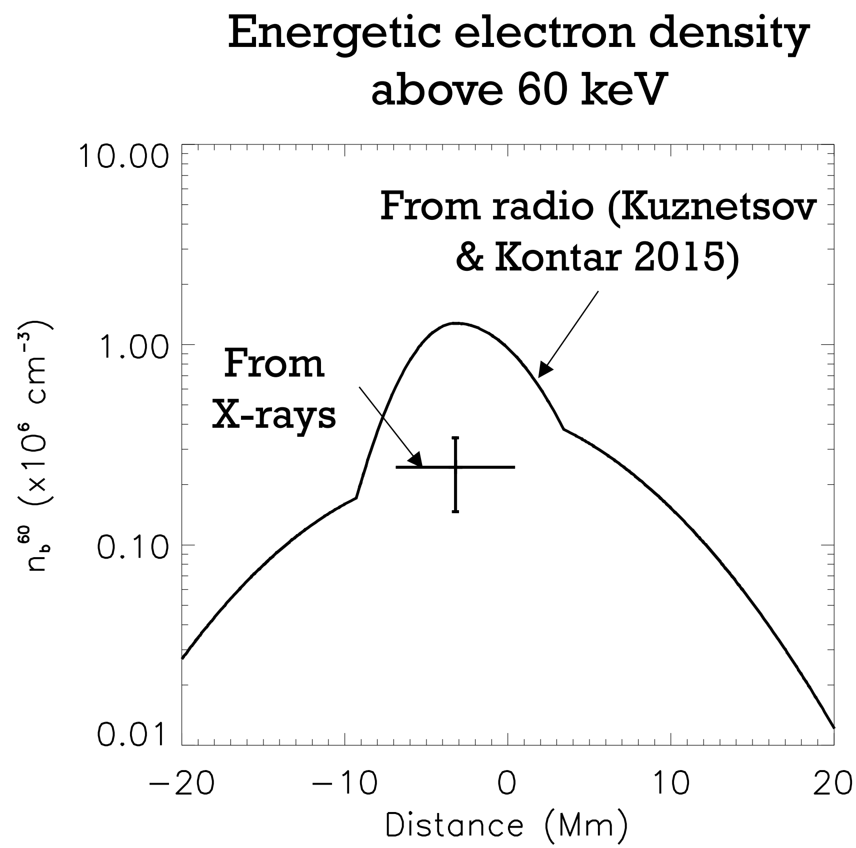

THE 2004 MAY 21 SOLAR FLARE

Energetic electron density above E_{min}

$$n_b^{E_{min}} = \int_{E_{min}}^{\infty} \frac{F(E)}{v(E)} dE \quad \text{cm}^{-3}$$

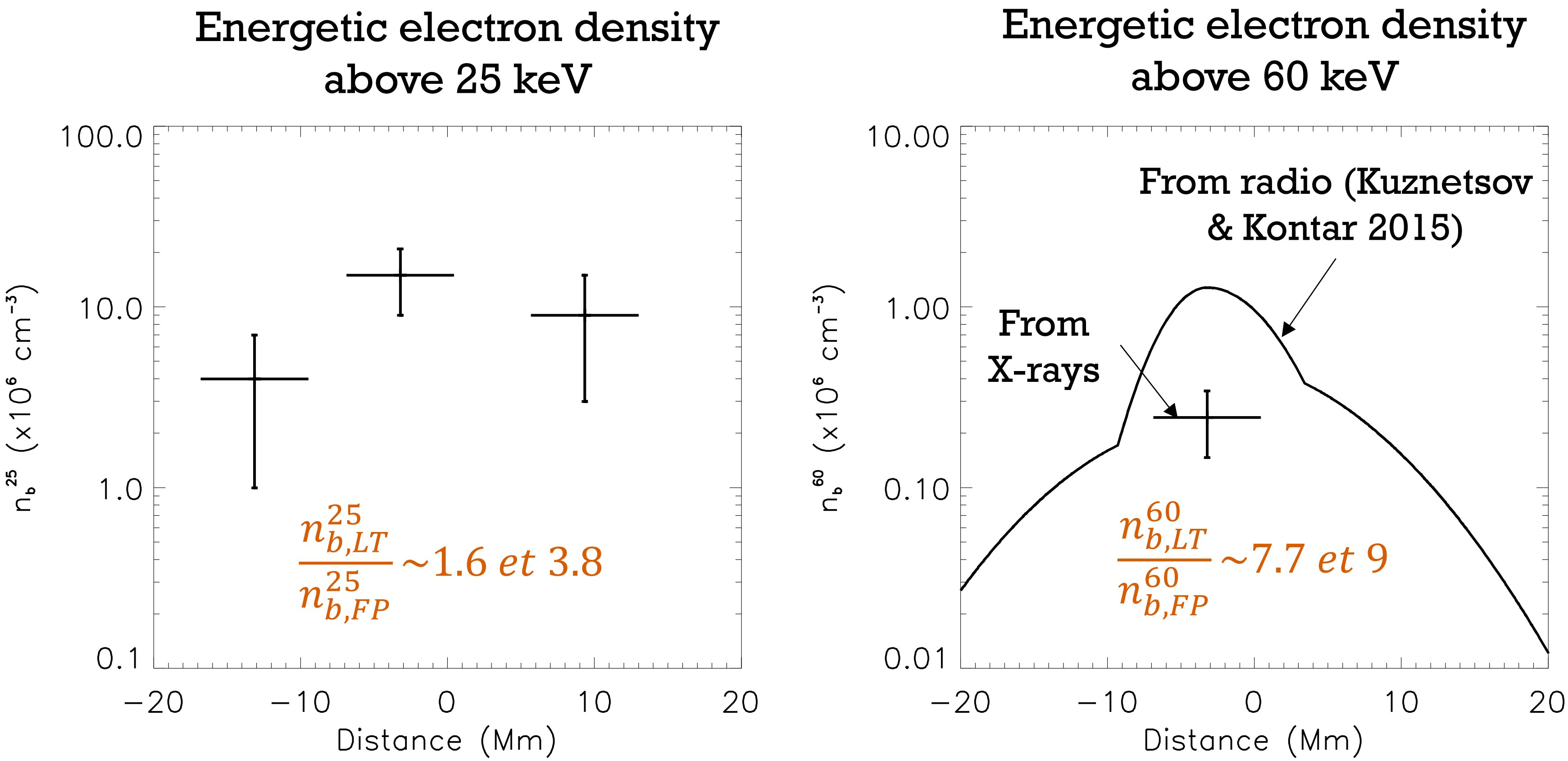

Distribution deduced from gyrosynchrotron emission is more peaked than the distribution deduced from X-rays

THE DIFFUSIVE TRANSPORT MODEL

Kontar et al (2014)

$$\frac{1}{v}\frac{\partial}{\partial z}\left(D_{zz}^{(T)}\frac{\partial F}{\partial z}\right) = \frac{\partial}{\partial E}\left(\frac{dE}{dx}F\right) + F_0 S(z)$$

Diffusion Collisions Source

$$D_{zz}^{(T)} = \frac{\lambda v}{3}$$

λ : mean free path

Strong pitch angle scattering due to small scale magnetic fluctuations
➔ diffusive transport of energetic electrons

THE DIFFUSIVE TRANSPORT MODEL

Kontar et al (2014)

$$\frac{1}{v}\frac{\partial}{\partial z}\left(D_{zz}^{(T)}\frac{\partial F}{\partial z}\right)=\frac{\partial}{\partial E}\left(\frac{dE}{dx}F\right)+F_0 S(z)$$

Diffusion Collisions Source

$$D_{zz}^{(T)}=\frac{\lambda v}{3}$$

λ : mean free path

Suppose λ constant

$$F_D(E,z)=\frac{E}{Kn_0}\int_E^{\infty}dE'\frac{F_0(E')}{\sqrt{4\pi a\left(E'^2-E^2\right)+2d^2}}\exp\left(-\frac{z^2}{4a\left(E'^2-E^2\right)+2d^2}\right)$$

$in\ electrons/cm^2/s/keV$

THE DIFFUSIVE TRANSPORT MODEL

Kontar et al (2014)

$$\frac{1}{v}\frac{\partial}{\partial z}\left(D_{zz}^{(T)}\frac{\partial F}{\partial z}\right) = \frac{\partial}{\partial E}\left(\frac{dE}{dx}F\right) + F_0 S(z)$$

Diffusion   Collisions   Source

$$D_{zz}^{(T)} = \frac{\lambda v}{3}$$

λ : mean free path

Suppose λ constant

$$F_D(E,z) = \frac{E}{K\boldsymbol{n_0}}\int_E^{\infty} dE' \frac{\boldsymbol{F_0}(E')}{\sqrt{4\pi\boldsymbol{a}\left(E'^2 - E^2\right) + 2\boldsymbol{d}^2}} \exp\left(-\frac{z^2}{4\boldsymbol{a}\left(E'^2 - E^2\right) + 2\boldsymbol{d}^2}\right)$$

$\boldsymbol{n_0}$ density of the medium
$\boldsymbol{d}$ size of the acceleration region
$\boldsymbol{a}$ α λ/n_0
$\boldsymbol{F_0}$ injected electron spectrum

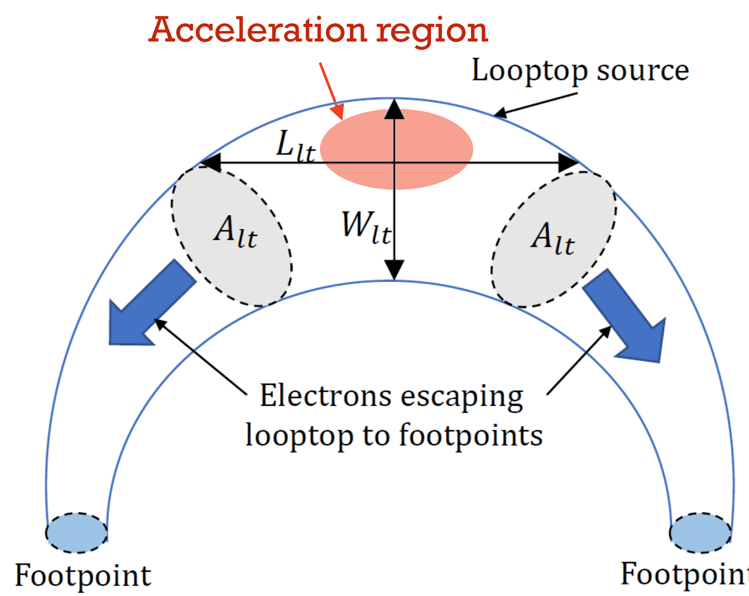

THE DIFFUSIVE TRANSPORT MODEL

Kontar et al (2014)

$$\frac{1}{v}\frac{\partial}{\partial z}\left(D_{zz}^{(T)}\frac{\partial F}{\partial z}\right) = \frac{\partial}{\partial E}\left(\frac{dE}{dx}F\right) + F_0 S(z)$$

Diffusion Collisions Source

$$D_{zz}^{(T)} = \frac{\lambda v}{3}$$

λ : mean free path

$$F_D(E,z) = \frac{E}{K\boldsymbol{n_0}}\int_E^{\infty} dE' \frac{\boldsymbol{F_0}(E')}{\sqrt{4\pi \boldsymbol{a}\left(E'^2 - E^2\right) + 2\boldsymbol{d}^2}} \exp\left(-\frac{z^2}{4\boldsymbol{a}\left(E'^2 - E^2\right) + 2\boldsymbol{d}^2}\right)$$

Spatial distribution of electrons at 20 keV

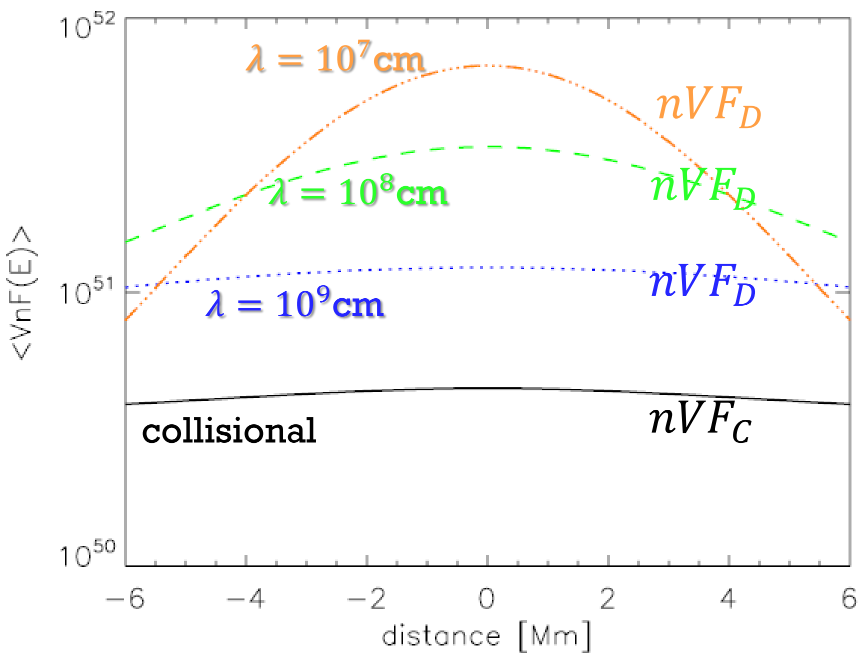

THE DIFFUSIVE TRANSPORT MODEL

Kontar et al (2014)

$$\frac{1}{v}\frac{\partial}{\partial z}\left(D_{zz}^{(T)}\frac{\partial F}{\partial z}\right) = \frac{\partial}{\partial E}\left(\frac{dE}{dx}F\right) + F_0 S(z) \qquad D_{zz}^{(T)} = \frac{\lambda v}{3}$$

Diffusion Collisions Source

λ : mean free path

$$F_D(E,z) = \frac{E}{K\boldsymbol{n_0}}\int_E^{\infty} dE' \frac{\boldsymbol{F_0}(E')}{\sqrt{4\pi \boldsymbol{a}(E'^2 - E^2) + 2\boldsymbol{d}^2}} \exp\left(-\frac{z^2}{4\boldsymbol{a}(E'^2 - E^2) + 2\boldsymbol{d}^2}\right)$$

Spatial distribution of electrons at 20 keV

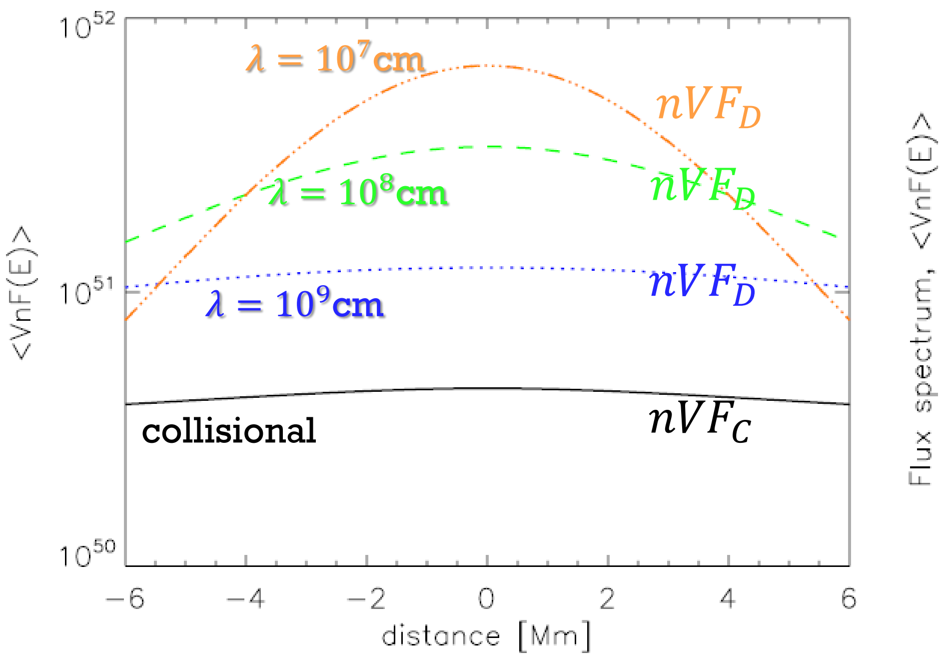

Looptop and footpoint spectra

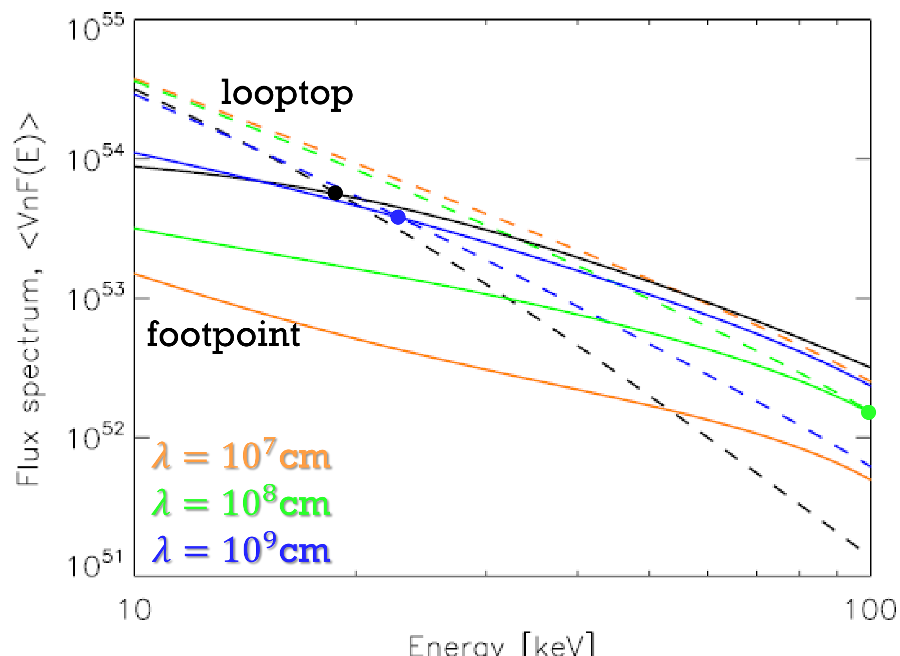

COMPARISON MODEL - OBSERVATIONS

Spatial distribution at 25 keV

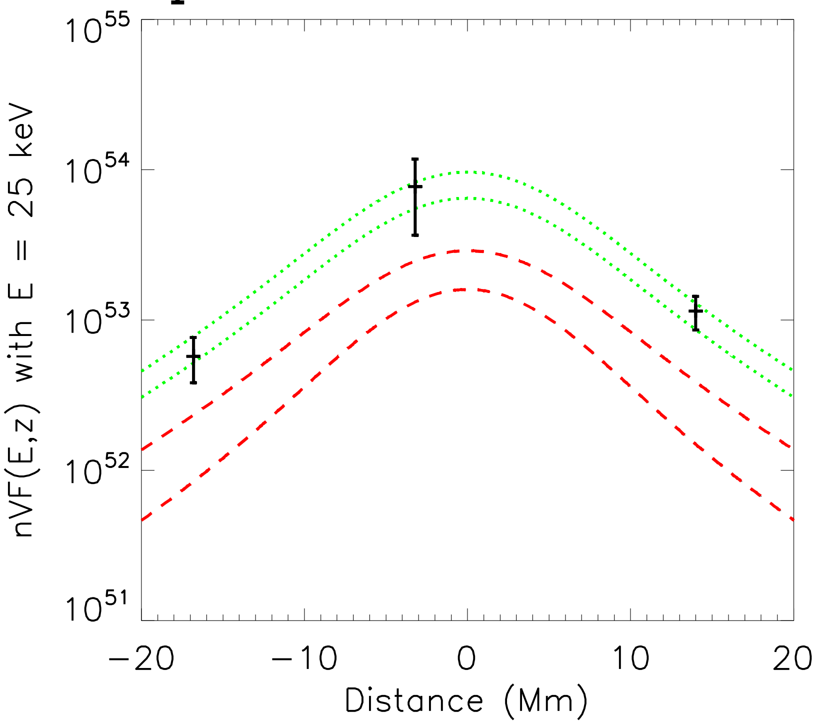

Coronal and footpoint spectra

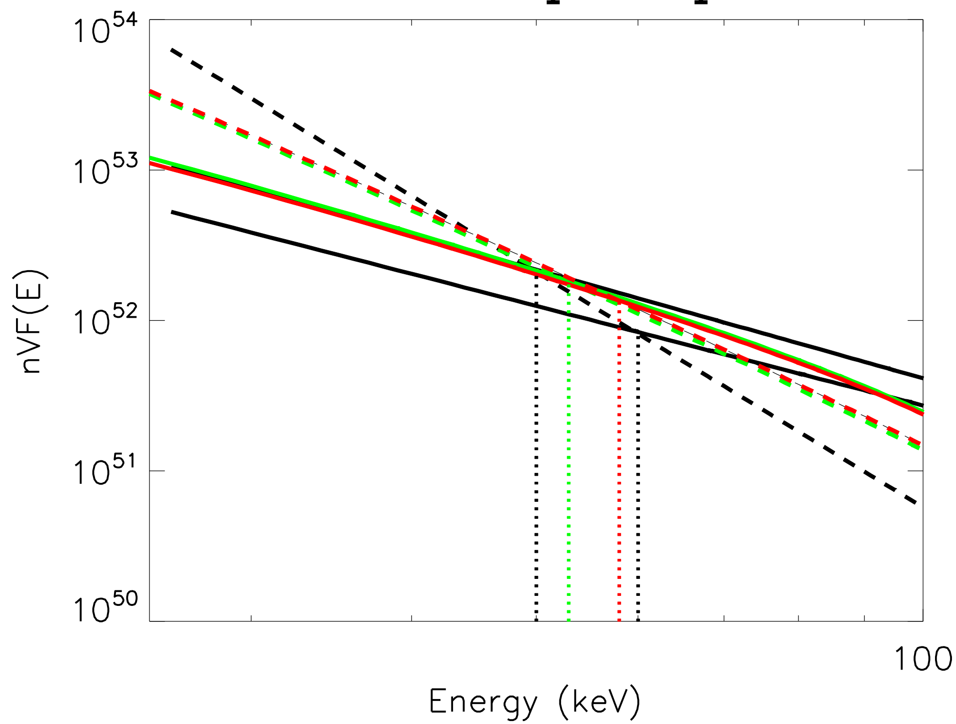

$n = 1.2 \pm 0.2 \times 10^{11}\ cm^{-3}$; $\lambda = 10^{9}\ cm$; $d = 3 \times 10^{8}\ cm$

$n = 3 \times 10^{10}\ cm^{-3}$; $\lambda = 3 \times 10^{8}\ cm$; $d = 3 \times 10^{8}\ cm$

λ Mean free path

d Size of acceleration region

$L \sim 3.2 \times 10^{9}$ cm

Length of the loop

COMPARISON MODEL - OBSERVATIONS

Spatial distribution of energetic electron density with energy > 25 keV

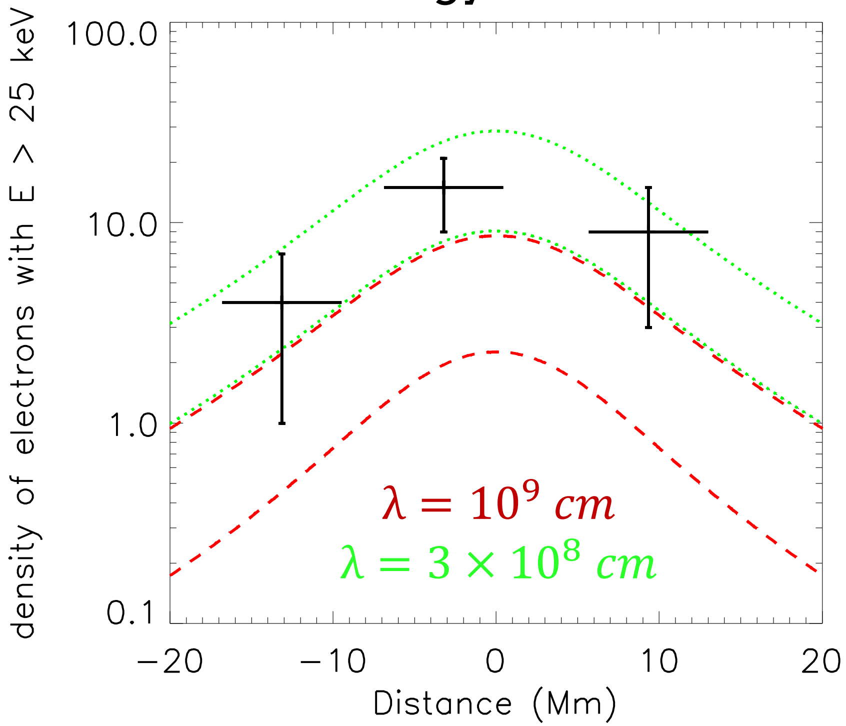

$n = 1.2 \pm 0.2 \times 10^{11}\ cm^{-3}$; $d = 3 \times 10^8\ cm$

$n = 3 \times 10^{10}\ cm^{-3}$; $d = 3 \times 10^8\ cm$

COMPARISON MODEL - OBSERVATIONS

Spatial distribution of energetic electron density
with energy > 25 keV

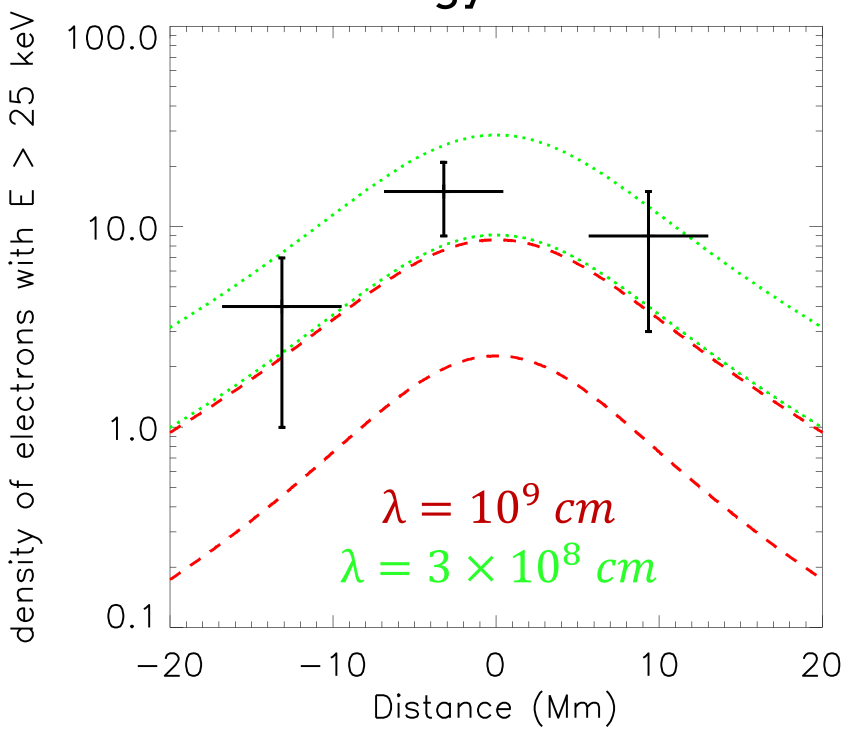

The diffusive transport model (Kontar et al. 2014) is consistent with the X-ray observations (spectral and spatial distribution).

What about the radio observations of Kuznetsov and Kontar (2015) ?

$n = 1.2 \pm 0.2 \times 10^{11}\ cm^{-3}\ ; d = 3 \times 10^8\ cm$

$n = 3 \times 10^{10}\ cm^{-3}\ ; d = 3 \times 10^8\ cm$

COMPARISON MODEL - OBSERVATIONS

Spatial distribution of energetic electron density

with energy > 25 keV

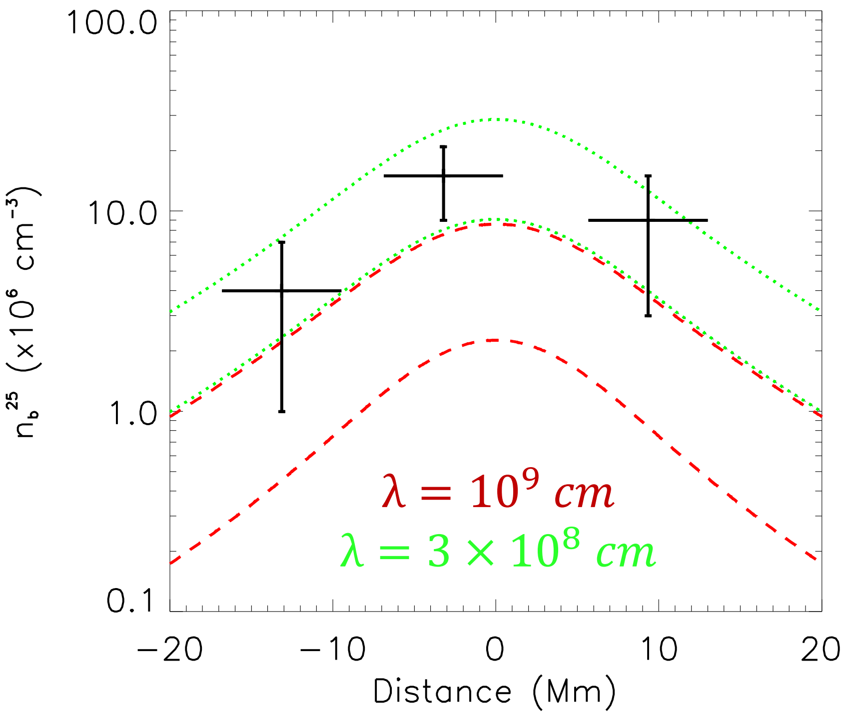

with energy > 60 keV

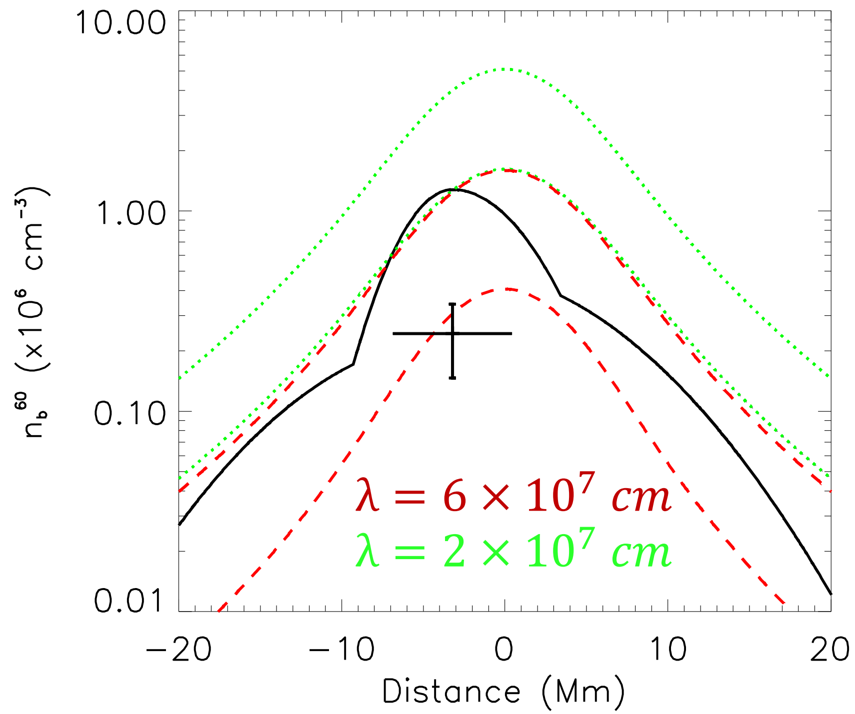

$n = 1.2 \pm 0.2 \times 10^{11}\ cm^{-3}$; $d = 3 \times 10^8\ cm$

$n = 3 \times 10^{10}\ cm^{-3}$; $d = 3 \times 10^8\ cm$

The distribution is more peaked: need a smaller λ

ALTERNATIVE: MAGNETIC MIRRORING

Trapping can be caused by magnetic field convergence.
The trapped fraction of particles is

$$T = 1 - \frac{\dot{N}_{FP}}{\dot{N}_{LT}}$$

And in the case of isotropic pitch-angle distribution, $T = \cos(\alpha_0)$
Where α_0 is the loss cone angle

$$\alpha_0 = \sin^{-1}(\sqrt{1/\sigma})$$

With $\sigma = B_{FP}/B_{LT}$ the magnetic ratio.
(Simoes & Kontar 2013)

ALTERNATIVE: MAGNETIC MIRRORING

Trapping can be caused by magnetic field convergence.
The trapped fraction of particles is

$$T = 1 - \frac{\dot{N}_{FP}}{\dot{N}_{LT}}$$

And in the case of isotropic pitch-angle distribution, $T = \cos(\alpha_0)$
Where α_0 is the loss cone angle

$$\alpha_0 = \sin^{-1}(\sqrt{1/\sigma})$$

With $\sigma = B_{FP}/B_{LT}$ the magnetic ratio.
(Simoes & Kontar 2013)

$$\frac{\dot{\boldsymbol{N}}_{\boldsymbol{FP}}}{\dot{\boldsymbol{N}}_{\boldsymbol{LT}}} = \mathbf{2.2} \;\Rightarrow\; \boldsymbol{\sigma} = \mathbf{1.4}$$

ALTERNATIVE: MAGNETIC MIRRORING

Trapping can be caused by magnetic field convergence.
The trapped fraction of particles is

$$T = 1 - \frac{\dot{N}_{FP}}{\dot{N}_{LT}}$$

And in the case of isotropic pitch-angle distribution, $T = \cos(\alpha_0)$
Where α_0 is the loss cone angle

$$\alpha_0 = \sin^{-1}(\sqrt{1/\sigma})$$

With $\sigma = B_{FP}/B_{LT}$ the magnetic ratio.
(Simoes & Kontar 2013)

$$\frac{\dot{N}_{FP}}{\dot{N}_{LT}} = 2.2 \quad \Rightarrow \quad \sigma = 1.4$$

Magnetic field strength along the loop (Kuznetsov & Kontar 2015)

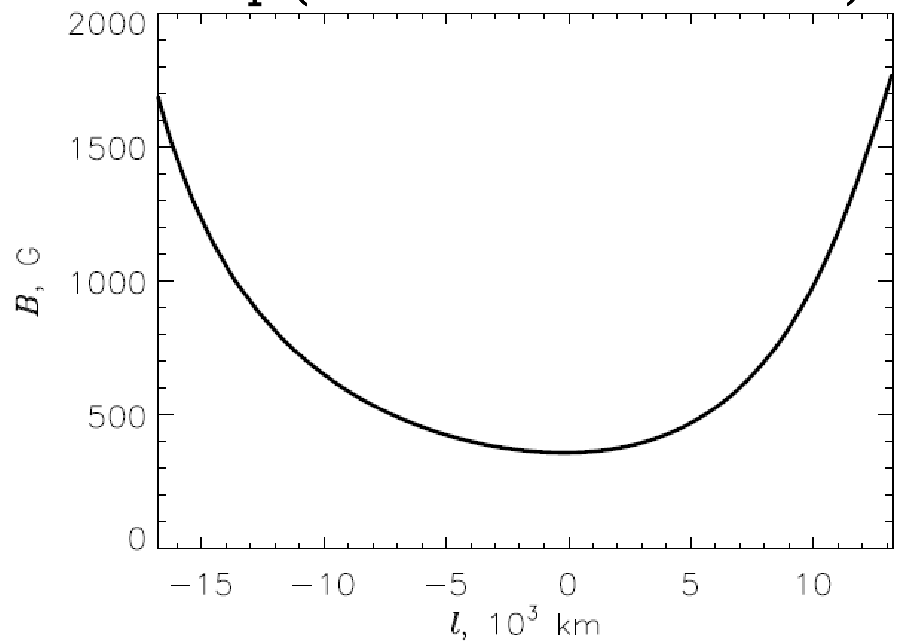

$$1.4 < \sigma < 4.7$$

ALTERNATIVE: MAGNETIC MIRRORING

Trapping can be caused by magnetic field convergence.
The trapped fraction of particles is

$$T = 1 - \frac{\dot{N}_{FP}}{\dot{N}_{LT}}$$

And in the case of isotropic pitch-angle distribution, $T = \cos(\alpha_0)$
Where α_0 is the loss cone angle

$$\alpha_0 = \sin^{-1}(\sqrt{1/\sigma})$$

With $\sigma = B_{FP}/B_{LT}$ the magnetic ratio.
(Simoes & Kontar 2013)

$$\frac{\dot{N}_{FP}}{\dot{N}_{LT}} = 2.2 \Rightarrow \sigma = 1.4$$

Magnetic field strength along the loop (Kuznetsov & Kontar 2015)

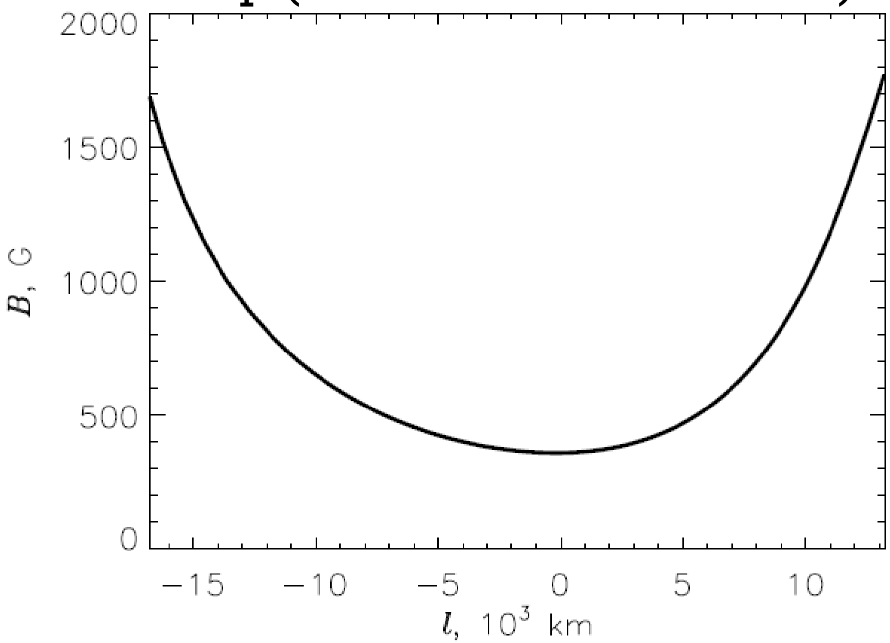

$$\mathbf{1.4 < \sigma < 4.7}$$

But how to explain the spectral hardening in the footpoints?

CONCLUSIONS

- ✓ Imaging spectroscopy is used to study the spatial distribution of electrons and the comparison of spectral distribution in different parts of the loop
- ✓ Diffusive transport model (Kontar et al 2014) can explain the X-ray observations
- ✓ Diffusive transport model can also explain the gyrosynchrotron observations, but with a smaller mean free path
  - ➔ Mean free path is energy dependant
- ✓ First comparison between radio and X-ray observations to probe energetic electrons trapping in the corona
  - ➔ Allows to probe two energy domains

CONCLUSIONS

- ✓ Imaging spectroscopy is used to study the spatial distribution of electrons and the comparison of spectral distribution in different parts of the loop
- ✓ Diffusive transport model (Kontar et al 2014) can explain the X-ray observations
- ✓ Diffusive transport model can also explain the gyrosynchrotron observations, but with a smaller mean free path
  - ➔ Mean free path is energy dependant
- ✓ First comparison between radio and X-ray observations to probe energetic electrons trapping in the corona
  - ➔ Allows to probe two energy domains

- ➢ Need to further develop the diffusive transport model with energy-dependent mean free path, and for relativistic electrons
- ➢ With imaging spectroscopy, model predictions about the spatial evolution of the electron distribution are useful to compare to observations